Semiclassical quantization of chaos in terms of an amplitude-free quasi-correlation function

2003 J. Phys. A: Math. Gen. 36 4785

(http://iopscience.iop.org/0305-4470/36/17/306)

INSTITUTE OF PHYSICS PUBLISHING JOURNAL OF PHYSICS A: MATHEMATICAL AND GENERAL

J. Phys. A: Math. Gen. **36** (2003) 4785–4803 PII: S0305-4470(03)52723-8

Semiclassical quantization of chaos in terms of an amplitude-free quasi-correlation function

Koji Hotta and Kazuo Takatsuka

Department of Basic Science, Graduate School of Arts and Sciences, The University of Tokyo, 153-8902, Tokyo, Japan

E-mail: hotta@mns2.c.u-tokyo.ac.jp and kaztak@mns2.c.u-tokyo.ac.jp

Received 21 August 2002, in final form 7 March 2003
Published 16 April 2003
Online at stacks.iop.org/JPhysA/36/4785

Abstract

A simple and practical semiclassical method based on an amplitude-free quasi-correlation function is proposed to quantize the energy spectrum of classically chaotic systems. Since classical trajectories used in this function are required to satisfy only a simple condition, the present method can be readily applied to a relatively large system. Numerical examples, which compare the semiclassical spectra with those of the full quantum mechanics in a two-dimensional system covering the regular and highly chaotic energy regions, show very clearly that the proposed amplitude-free quasi-correlation function can quantize chaos surprisingly well.

PACS numbers: 05.45.Mt, 03.65.Sq, 33.20.Tp, 36.40.−c

1. Introduction

The quantization of the energy spectrum in chaotic classical systems and the investigation of its mechanism remain one of the most fundamental issues in quantum chaos [1, 2]. Gutzwiller's periodic orbit theory [3] opened a new era of quantum chaos. The theory treats the density of states with the semiclassical Feynman kernel $K_{\rm sc}$ as

$$D(E) = \int \mathrm{d}q \int \mathrm{d}t\, K_{\rm sc}(q, q, t) \exp\left(\frac{\mathrm{i}}{\hbar} Et\right) \tag{1}$$

and the successive applications of the stationary phase approximations to $D(E)$ lead to an expression

$$D(E) \simeq \frac{1}{(2\pi\hbar)^N} \int\int \mathrm{d}q\, \mathrm{d}p \delta(E - H_{\rm cl}(q, p)) + \frac{1}{\pi\hbar} \sum_{\gamma} \sum_{k=1}^{\infty} \frac{T_\gamma \cos\left(k\left(\frac{W_\gamma}{\hbar} - \frac{\pi}{2}\lambda_\gamma\right)\right)}{\sqrt{\left|\mathrm{Det}\left(M_\gamma^k - I\right)\right|}} \tag{2}$$

where the first term on the right-hand side is the well-known Thomas–Fermi density of states based on the classical Hamiltonian $H_{\rm cl}(q, p)$, and the second oscillatory terms represent the

quantum interference among the periodic orbits (specified by γ) in terms of the period T_γ, the action integral W_γ, and the monodromy matrix M_γ^k in the transversal direction of phase-space periodic motion. These terms should be summed up with respect to the times of repetition k over all the possible periodic orbits. Although this theory is very clear and still of central importance, the following difficulties are widely recognized. (1) In chaotic systems, the periodic orbits emanate almost exponentially with the period. (2) It is extremely difficult to pick those periodic orbits even in two-dimensional generic systems. (3) The periodic orbit expansion is not absolutely convergent in practice. In the literature, many endeavours have been devoted to overcoming these difficulties. For instance, Voros [4] and Berry and Keating [5] developed theories to improve the convergence property. Very recently, Vergini *et al* [6] have demonstrated the dominance of short periodic orbits to generate chaotic wavefunctions in terms of resonant basis functions. Nevertheless, the quantization of chaos within the framework of *strictly* periodic orbits is still far from the practical level[1].

A natural alternative to the periodic orbit theory is to return to the straightforward evaluation of the correlation function using the semiclassical kernel

$$K_{\rm sc}(q, q_0, t) = (2\pi {\rm i}\hbar)^{-N/2} \int \delta(q - q_t) \left| \frac{\partial q_t}{\partial p_0} \right|^{\frac{1}{2}} \exp\left(\frac{\rm i}{\hbar} S(q_t, q_0, t) - {\rm i}\pi \frac{\lambda}{2} \right) {\rm d}p_0 \tag{3}$$

in a wavepacket dynamics $\phi(t)$ as

$$\langle \phi(0) | \phi(t) \rangle = (2\pi {\rm i}\hbar)^{-N/2} \int \phi^*(q_t)\phi(q_0) \left| \frac{\partial q_t}{\partial p_0} \right|^{1/2} \exp\left(\frac{\rm i}{\hbar} S(q_t, q_0, t) - {\rm i}\pi \frac{\lambda}{2} \right) {\rm d}q_0\, {\rm d}p_0 \tag{4}$$

the Fourier transform of which should give a relevant spectrum. This direct approach does not specify the geometry of trajectories and hence seems very powerful. All we need to do is to run as many *anonymous* trajectories as possible. The kernel in equation (3) is called the initial value representation (IVR) [7–11], which makes it possible to launch trajectories with the initial conditions $(q_0,\ p_0)$ in phase space and removes the well-known singularity $|\partial q_t/\partial p_0|^{-1/2} = \infty$ at caustics [12]. We refer to this method as the K-IVR in what follows. However, a fatal difficulty is hidden behind equation (4) [13]: the amplitude factor $|\partial q_t/\partial p_0|^{1/2}$ in equation (4) undergoes an exponential increase (divergence) in a manner of $|\partial q_t/\partial p_0|^{\frac{1}{2}} \sim \exp(\bar{K}t/2)$, where $\bar{K}$ is an average of the local K-entropy [14] of a trajectory. $\bar{K}$ becomes positive and larger as chaos becomes stronger. This type of spurious divergence is basically shared by other semiclassical theories. Thus, in a strongly chaotic system having a large $\bar{K}$, the semiclassical correlation function practically gives not delta-function spikes in the energy spectrum but at most only Lorentzian peaks with a bad resolution, as will be exemplified later in section 3.2 in order to confirm the level of accuracy of equation (4).

It is thus widely recognized that the difficulty in semiclassical quantization originates from the amplitude factor in the kernel. Recently, we have formulated a semiclassical quasi-correlation function that is not associated with the amplitude factor [15]. We call it the amplitude-free quasi-correlation function of type I (AFC-I). Since the AFC-I is represented in terms of what we call turn-back orbits (see equation (26) for the definition), which are very easy to generate, it can be applied for the quantization of large chaotic systems practically. In section 3.3 we show numerical examples of the AFC-I spectra to compare the full quantum (FQ) spectra for some selected cases including regular, weakly chaotic, and strongly chaotic systems. It turns out that the AFC-I produces the spectral lines at correct positions (energies) very well, but also the resultant spectrum is contaminated with rather strong noises.

[1] By 'practical level', we mean practical quantization of chaos for general potentials, which are not as simple as the stadium billiard, of more than two degrees of freedom.

Analysing the noises in the AFC-I spectra, we have found that the AFC should efficiently pick those special turn-back orbits that are weakly periodic (turn-back orbit with weak periodicity). Thus, we have reformulated the AFC-I so as to take account of the weak periodicity in an efficient manner without searching for the *strictly* periodic orbits. The reformulated quasi-correlation function is called AFC-II. Its technical advantages, freedom from the diverging amplitude factor and easy generation of the turn-back orbits, are all maintained. The numerical test using the common systems to the kernel and AFC-I reveals that the AFC-II gives surprisingly sharp and correct spectra with low noises. Thus it turns out that the AFC-II provides a very promising approach for quantization of large systems. We also discuss the basic properties and remaining difficulty of the AFC-II.

The present paper is organized as follows. In section 2, we outline the semiclassical theory (action decomposed function) and the AFC-I based on it. Prior to the presentation of the spectra of the AFC-I, we show, in section 3, the exponential increase of the correlation function and the resultant spectra calculated with the K-IVR of equation (4). This will provide a standard with which to judge the level of performance of other semiclassical theories. We then proceed to test the AFC-I using the common system. Although the situation is drastically improved, AFC-I turns out to be contaminated with strong noise. We reformulate the AFC-I in section 4 in order to suppress the noise, demonstrating the dramatic performance of the AFC-II. We conclude the paper in section 5 with some remarks.

2. Action decomposed function and AFC-I

We summarize the action decomposed function (ADF) [16] and associated AFC [15] in this section.

2.1. Action decomposed function

Our semiclassical argument begins with the ADF of the following form

$$\Psi_{p_0}(q,t) = F(q,t)\exp\left[\frac{\mathrm{i}}{\hbar}S_2(q,\,p_0,t)\right] \tag{5}$$

which is to be propagated in terms of the equation of motion of the lowest order approximation in $\hbar$ to the Schrödinger equation. S_2 is the classical action that satisfies the Hamilton–Jacobi equation of the F_2 type generating the function of Goldstein [17]. Hence the initial form of $\Psi_{p_0}(q,t)$ is

$$\Psi_{p_0}(q,0) = F(q,0)\exp\left[\frac{\mathrm{i}}{\hbar}p_0 q\right]. \tag{6}$$

The function $F(q,t)$ is determined by the following equation of motion

$$\frac{\partial F}{\partial t} + v\cdot\nabla F = -\frac{1}{2}(\nabla\cdot v)F \tag{7}$$

where $v(t) = \partial S_2(q,\,p_0,t)/\partial q$ is the classical velocity. We use the mass-weighted coordinates throughout so that all the masses are scaled to unity. Equation (7) is integrated as follows. We start from the following observation:

$$\frac{\partial F^2}{\partial t} + \nabla\cdot(vF^2) = 0. \tag{8}$$

Note that F^2 rather than $|F|^2$ is considered in this 'equation of continuity' (notice that F^2 can be complex). F^2 can be readily integrated locally along classical paths in terms of a Jacobian

determinant $\partial q_t/\partial q_0$ which is a minor determinant of the so-called stability matrix. It is not difficult to derive the equation

$$\frac{\partial}{\partial t}\left(\frac{\partial q_t}{\partial q_0}\right)^{-1} + \nabla\cdot\left(v\left(\frac{\partial q_t}{\partial q_0}\right)^{-1}\right) = 0 \tag{9}$$

from the Hamilton–Jacobi equation for $S_2(q_t, p_0, t)$. Furthermore, we have the initial condition $(\partial q_t/\partial q_0)^{-1} = 1$, since $q_t = q_0$ at $t = 0$. Thus $(\partial q_t/\partial q_0)^{-1}$ can be regarded as a local representation of the Green function for the propagator of equation (8). On comparing equations (8) and (9), together with the initial conditions above, we immediately have

$$F(q_t, t) = F(q_0, 0)\left(\frac{\partial q_t}{\partial q_0}\right)^{-\frac{1}{2}} = F(q_0, 0)\left|\frac{\partial q_t}{\partial q_0}\right|^{-\frac{1}{2}}\exp\left[-\frac{\mathrm{i}\pi M(q_0, q_t)}{2}\right] \tag{10}$$

where the derivative $\partial q_t/\partial q_0$ is taken under the fixed initial momentum p_0, and $M(q_0, q_t)$ is the Maslov index in this representation which counts the number of zeroes of $\partial q_t/\partial q_0$ up to the degeneracy. Thus the local solution, denoted by $\Psi^{p_0}_{\mathrm{local}}(q_t, t)$, is evolved in time on an action surface, which is in turn to be propagated in terms of trajectories of a fixed initial momentum p_0. The final expression for the wavefunction is then written as

$$\begin{aligned}\Psi_{p_0}(q, t) &= \int \delta(q - q_t)\Psi_{p_0}(q_t, t)\,\mathrm{d}q_t \\ &= \int \delta(q - q_t(q_0, p_0))F(q_0, 0)\left|\frac{\partial q_t}{\partial q_0}\right|^{\frac{1}{2}}\exp\left[\frac{\mathrm{i}}{\hbar}S_2(q_t, p_0, t) - \frac{\mathrm{i}\pi M(q_0, q_t)}{2}\right]\mathrm{d}q_0\end{aligned} \tag{11}$$

which will be used to make the auto-correlation function.

2.2. Square root of volume elements in semiclassical integrals

To treat the transformation among the semiclassical integrals systematically, we consider a rather general multi-dimensional integral

$$I = \int f(q_0)\,\mathrm{d}q_0 = \int f(q_t)\left|\frac{\partial q_0}{\partial q_t}\right|\mathrm{d}q_t. \tag{12}$$

In this expression, we should note that the small volume element $\mathrm{d}q_t$ can be an oriented volume with respect to $\mathrm{d}q_0$, the sign of which is represented in terms of that of the Jacobian determinant $\partial q_t/\partial q_0$, since the volume can be inverted in many ways in addition to the change in its shape and volume. Let us define the square root of the volume elements of the integral [15] such that

$$I = \int f(q_0)\,\mathrm{d}q_0^{\frac{1}{2}}\,\mathrm{d}q_0^{\frac{1}{2}*} \tag{13}$$

where $\mathrm{d}q_0^{\frac{1}{2}*}$ is the complex conjugate of $\mathrm{d}q_0^{\frac{1}{2}}$. The positive semidefinite quantity $\mathrm{d}q_0$ ($\mathrm{d}q_t$) is understood to be a product

$$\mathrm{d}q_0 \equiv |\mathrm{d}q_0| = \mathrm{d}q_0^{\frac{1}{2}}\,\mathrm{d}q_0^{\frac{1}{2}*} \quad \text{and} \quad \mathrm{d}q_t \equiv |\mathrm{d}q_t| = \mathrm{d}q_t^{\frac{1}{2}}\,\mathrm{d}q_t^{\frac{1}{2}*}. \tag{14}$$

As in the ordinary complex numbers, the square of $\mathrm{d}q_t^{\frac{1}{2}}$ is not equal to $\mathrm{d}q_t$ unless the former is real-valued. We now define $\mathrm{d}q_t^{\frac{1}{2}}$ as

$$\mathrm{d}q_t^{\frac{1}{2}} = \exp\left[\mathrm{i}\frac{\pi}{2}N(q_t)\right]|\mathrm{d}q_t|^{\frac{1}{2}} \tag{15}$$

where $N(q_t)$ is the sum of zeros up to the degeneracy of the following determinant picked up by a Jacobian determinant

$$\frac{\partial q_t}{\partial q_{t=X}} \tag{16}$$

along a path. It is convenient to set the reference of time $t = X$ at a far remote past, symbolically denoted as $X = -\infty$. With these quantities, the conservation rule including the phase can be rewritten in a compact form as

$$F(q_t, t)\,\mathrm{d}q_t^{\frac{1}{2}} = F(q_0, 0)\,\mathrm{d}q_0^{\frac{1}{2}} \tag{17}$$

which is valid when the two points are connected by a trajectory. In fact, equation (17) comes back to

$$F(q_t, t)\exp\left[\mathrm{i}\frac{\pi}{2}N(q_t)\right]|\mathrm{d}q_t|^{\frac{1}{2}} = F(q_0, 0)\exp\left[\mathrm{i}\frac{\pi}{2}N(q_0)\right]|\mathrm{d}q_0|^{\frac{1}{2}} \tag{18}$$

giving the Maslov index

$$M(q_0, q_t) = N(q_t) - N(q_0). \tag{19}$$

2.3. AFC-I

Rewriting the ADF of equation (11) as

$$\Psi_{p_0}(q, t) = \int \delta(q - q_t)\exp\left[\frac{\mathrm{i}}{\hbar}S_2(q_t, p_0, t)\right]F(q_0, 0)\,\mathrm{d}q_0^{\frac{1}{2}}\,\mathrm{d}q_t^{\frac{1}{2}*} \tag{20}$$

we study the following correlation function

$$\begin{aligned} C_{p_0}(-t, t) &= \langle\Psi_{p_0}(-t)|\Psi_{p_0}(t)\rangle \\ &= \int\int \delta(q_{-t}-q_t)F^*(q_{01}, 0)F(q_{02}, 0)\exp\left[\frac{\mathrm{i}}{\hbar}S_1(q_t, q_{02}, t) + \frac{\mathrm{i}}{\hbar}p_0q_{02}\right. \\ &\quad \left. - \frac{\mathrm{i}}{\hbar}S_1(q_{-t}, q_{01}, -t) - \frac{\mathrm{i}}{\hbar}p_0q_{01}\right]\mathrm{d}q_{01}^{\frac{1}{2}*}\,\mathrm{d}q_{02}^{\frac{1}{2}}\,\mathrm{d}q_{-t}^{\frac{1}{2}}\,\mathrm{d}q_t^{\frac{1}{2}*} \end{aligned} \tag{21}$$

from which the energy spectrum is to be extracted. $S_1(q_t, q_0, t)$ is the ordinary F_1-type action integral [17]. It is easy to confirm $C_{p_0}(-t, t)^* = C_{p_0}(t, -t)$.

Equation (21) requires two trajectories to end up at the same point q_t with different initial points q_{01} and q_{02}, namely,

$$q_t(q_{02}, p_0) = q_{-t}(q_{01}, p_0) \tag{22}$$

where $q_t(q_{02}, p_0)$, for instance, indicates a position q_t reached by a trajectory at time t that started with an initial condition (q_{02}, p_0) at time $t = 0$. (Note that $q_{-t}(q_{01}, p_0) = q_t(q_{01}, -p_0)$.) Therefore, we have to search a pair of (q_{01}, q_{02}) satisfying equation (22) for given p_0 and t.

Next let us integrate $C_{p_0}(-t, t)$ over p_0 to pick spectral information as much as possible as

$$\begin{aligned} \int \mathrm{d}p_0 C_{p_0}(-t, t) &= (2\pi\hbar)^N \int\int \delta(q_{-t}-q_t)F^*(q_{01}, 0)F(q_{02}, 0)\delta(q_{01} - q_{02}) \\ &\quad \times \exp\left[\frac{\mathrm{i}}{\hbar}S_1(q_t, q_{02}, t) - \frac{\mathrm{i}}{\hbar}S_1(q_{-t}, q_{01}, -t)\right]\mathrm{d}q_{01}^{\frac{1}{2}*}\,\mathrm{d}q_{02}^{\frac{1}{2}}\,\mathrm{d}q_{-t}^{\frac{1}{2}}\,\mathrm{d}q_t^{\frac{1}{2}*} \end{aligned} \tag{23}$$

which gives the additional condition, that is

$$q_{01} = q_{02}. \tag{24}$$

Inserting this into equation (22), we have

$$q_t(q_{01}, p_0) = q_{-t}(q_{01}, p_0) = q_t(q_{01}, -p_0). \tag{25}$$

This condition can be generally satisfied by the following two classes of trajectories. (i) The periodic orbits satisfying $q_t(q_{01}, p_0) = q_{01}$ and $p_t(q_{01}, p_0) = p_0$, namely $(q_t, p_t) = (q_{01}, p_0)$. (ii) The turn-back orbits that satisfy

$$q_{-t} = q_t \qquad \text{via} \quad p_0 = 0 \tag{26}$$

(at any q_{01}) [15]. The geometrical meaning of the turn-back orbit is clear. It encounters the turning point at $t = 0$ (by satisfying $p_0 = 0$) and traces back along the same path to the same point ($q_{-t} = q_t$). Therefore, if the quantum phase via the action integral along the incoming trajectory ($t < 0$) can have a constructive interference with that of the reflective wave ($t > 0$), we can expect the formation of a standing wave on this trajectory. This is physically analogous to a waving motion of a string, one end of which is fixed on a wall and the other is shaken. We should, of course, study both the periodic and turn-back orbits. However, it is obvious that adopting the *strictly* periodic orbits brings this correlation function back into the difficult situations mentioned above. We therefore concentrate first on the turn-back orbits to estimate the correlation function, since they are far easier to generate (simply put $p_0 = 0$ at any point q_{01}).

In coping with the oscillatory integrals such as equation (23), we do not perform the stationary phase approximation faithfully, but we simply retain the turn-back orbits in $C_{p_0}(-t, t)$, neglecting all the contributions made by other paths. The additional amplitude factor arising from the second derivative of the phase factor is not evaluated in the present context. This is because the accurate evaluation of the absolute magnitude of the correlation function (or the power spectrum thereof) is not necessary. Only digital type information is required, which should give non-zero values at the positions of the eigenvalues and zero otherwise. Setting $q_{01} = q_{02}\,(=q_0)$ and $p_0 = 0$ in equation (21), we devised an AFC [15], which we here call AFC-I,

$$\tilde{C}_I(-t, t) = \int \mathrm{d}q_0 F^*(q_0, 0) F(q_0, 0) \exp\left[\frac{\mathrm{i}}{\hbar}\left(S_1(q_t, q_0, t) - S_1(q_{-t}, q_0, -t)\right) - \mathrm{i}\frac{\pi}{2} M(q_{-t}, q_t)\right] \tag{27}$$

where the Maslov index is to be calculated along the turn-back orbits $q_{-t} \to q_t$. The spectrum is to be extracted as

$$\begin{aligned} S(E) &= \mathrm{Re} \lim_{T\to\infty} \frac{2}{T} \int_0^{T/2} \tilde{C}_I(-t, t) \exp\left(2\frac{\mathrm{i}}{\hbar} Et\right) \mathrm{d}t \\ &= \lim_{T\to\infty} \frac{2}{T} \int_0^{T/2} \mathrm{d}t \int \mathrm{d}q_0 |F(q_0, 0)|^2 \cos\left[\frac{2}{\hbar} S_1(q_t, q_0, t) - \frac{\pi}{2} M(q_{-t}, q_t) + \frac{2}{\hbar} Et\right]. \end{aligned} \tag{28}$$

It is remarkable that the annoying amplitude factor, such as $|\partial q_t/\partial p_0|^{1/2}$ in equation (4) or $|\partial q_t/\partial q_0|^{1/2}$ in equation (11), is missing in this expression. This is because the amplitude factor $\partial q_t/\partial q_{-t}$ is always unity in the manifold of the turn-back orbits [15]. (For other AFCs, see [18, 19].) Recall that the amplitude factors diverge exponentially for a chaotic system. Note, on the other hand, that the Maslov index does remain in $\tilde{C}_I(-t, t)$ as an essential part of the quantum phase. We also note that $\tilde{C}_I(-t, t)$ is written in q-representation and the concept of turn-back orbit nor $\tilde{C}_I(-t, t)$ of equation (27) is canonically invariant (see below).

3. Numerical studies for AFC-I and K-IVR

We here present the numerical performance of the AFC-I, while the final goal of this paper is to propose a revised version of the AFC-I, namely the AFC-II, through the analysis of AFC-I. Prior to the presentation of AFC-I and II, we show some numerical examples of the exponential increase of the correlation function estimated with the K-IVR of equation (4) and associated spectra. The systems used for the test are all common to these semiclassical methods. They will clearly demonstrate how difficult the quantization of chaos is, and moreover the level of performance of AFC-I and AFC-II can be examined in an objective perspective. Although there can be various ways to reformulate the original semiclassical kernel to have a better performance, we do not survey these as this is out of our scope in this paper. Also, we could not carry out the Gutzwiller trace formula for comparison because of its technical difficulty.

3.1. Systems

The following two-dimensional modified Hénon–Heiles system [20]

$$H = \frac{p_x^2}{2m_x} + \frac{p_y^2}{2m_y} + \frac{x^2+y^2}{2} + x^2(0.6y^2 + y) + \frac{y^3}{3}(0.2y - 1) + Ax \tag{29}$$

with $m_x = 1.0087$ and $m_y = 1.0$ is used as a system to test the theories we are going to compare. Such a small mass imbalance was introduced before to break a certain phase-space structure but it has no significance in the present context. The last term Ax has been introduced to break the spatial symmetry with respect to the axis of $x = 0$. This system can become strongly chaotic with appropriate parameters and thereby gives a stringent test for the energy quantization of chaos.

As for the AFC, we choose $F(q_0, 0)$ in equations (6) and (28) to be the coherent-state Gaussian wavepacket of the minimum uncertainty

$$F(q, 0) = \exp\left[-\frac{1}{2\hbar}((x - x_0)^2 + (y - y_0)^2)\right] \tag{30}$$

(put $p_0 = 0$ in equation (6) for the turn-back orbits), while for the wavepacket in the K-IVR of equation (4) we use

$$\phi(q, 0) = \exp\left[-\frac{1}{2\hbar}((x - x_0)^2 + (y - y_0)^2) + \frac{\mathrm{i}}{\hbar}p_{x0}(x - x_0) + \frac{\mathrm{i}}{\hbar}p_{y0}(y - y_0)\right]. \tag{31}$$

The Planck constant is $\hbar = 0.005$. For the exact eigenvalues, we numerically integrate the Schrödinger equation to propagate $\phi(q, t)$ to compute the correlation function and associated spectra. The Kosloff FFT method [21] and the symplectic integrator [22] have been used to integrate the Schrödinger equation. The spectrum thus obtained is denoted as the FQ spectrum and is used for comparison throughout this paper.

With this Hamiltonian, the following three selected cases are to be studied.

(a) *Regular system:* We focus on the energy region around $E = 0.03$ for the Hamiltonian $A = 0$. See figure 1 for the Poincaré surface of the section taken at $x = 0$ with $p_x > 0$, showing that the phase space is mostly filled with the KAM tori.

(b) *Weakly chaotic system:* This system is characterized in terms of the so-called vague tori [23], at an energy region $E = 0.25$ with $A = 0$. The Poincaré section in figure 2 displays such an example of the time propagation of a vague torus, in which a trajectory that initially happens to be very close to the torus-like structure begins to leave and wander in the wider space of phase space after a long time. Other sampled trajectories may start

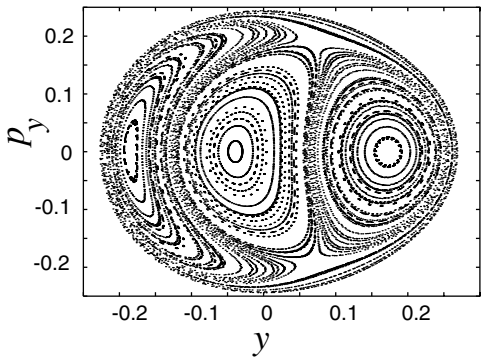

Figure 1. Classical Poincaré surface of section at $x = 0$, $p_x > 0$ at $E = 0.03$ for the potential $A = 0.0$. The system is filled with the KAM tori. (The absolute units are used throughout.)

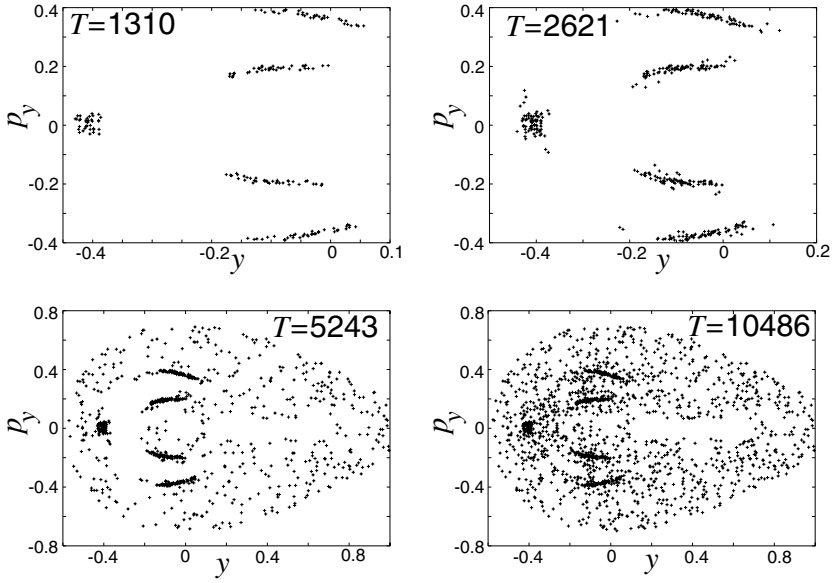

Figure 2. Classical Poincaré surface of section at $x = 0$, $p_x > 0$ at $E = 0.25$ for the potential $A = 0.0$. A time propagation of a broken torus.

from the chaotic sea. It should be noted that the vague (broken) tori are usually adjacent to the fully chaotic sea that lies in slightly higher energy phase space. Therefore, even if a quantum wavepacket is selected in such a way that its classical energy $(x_0, p_{x0}, y_0, p_{y0})$ is centred at $E = 0.25$, it may cover the higher energy area corresponding to very strong chaos.

(c) *Strongly chaotic system:* This is at an energy region around $E = 0.15$ in a slightly different Hamiltonian of $A = 0.1$. As shown in figure 3, the phase space is filled with chaotic sea almost everywhere.

3.2. Numerical study for the semiclassical kernel (K-IVR)

We first show the numerical examples of the time propagation of the correlation function of equation (4) and the resultant spectra extracted from them. The trajectories are sampled in

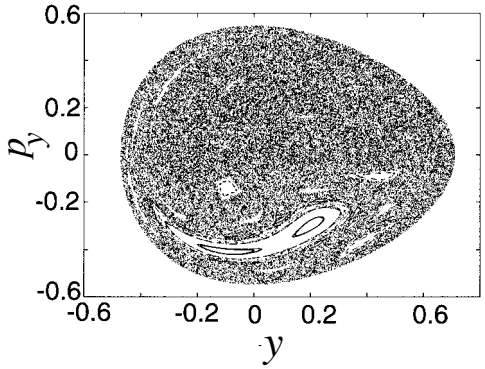

Figure 3. Classical Poincaré surface of section at $x = 0$, $p_x > 0$ at $E = 0.15$ for the potential $A = 0.1$. The system is almost fully chaotic.

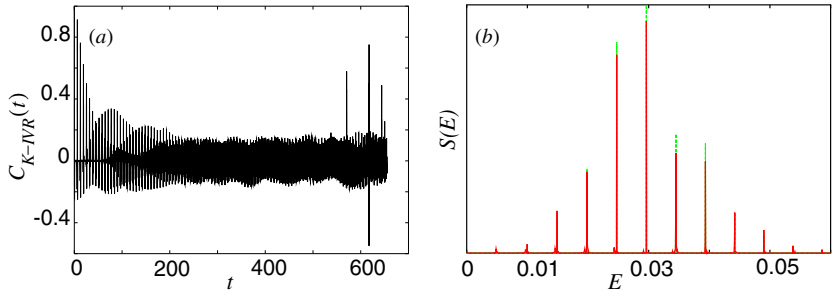

Figure 4. (*a*) The real part of the correlation function in the presence of the KAM around $E = 0.03$ for the Hamiltonian $A = 0.0$ with the number of samples trajectories $N_t = 10\,000$. (*b*) A close-up of the spectrum around $E = 0.03$ taken from the correlation function of (*a*) for the time interval $T = 655$. The spectral positions given by the K-IVR (red) and FQ (green) spectra are indistinguishable. (The absolute units are used throughout.)

q-space so as to mimic the Gaussian part of $\phi(q, 0)$ in equation (31), i.e. $|\phi(q, 0)|$, using the importance sampling technique. Although the correlation function of equation (4) requires us to sample the trajectories in a uniform distribution of the initial momentum p_0, we truncate the high kinetic energy components so that the energy distribution of thus sampled trajectories has a peak near the energy under study. Without such an artificial truncation, the divergence property of the correlation function is more violent.

(a) *Regular system:* The time evolution of the correlation function is shown in figure 4(*a*). It oscillates normally without divergent behaviour. The resultant semiclassical spectrum (the red curve in figure 4(*b*)) is well discretized at correct positions represented by the FQ spectrum in green. No difficulty arises in this case.

(b) *Weak chaos:* We next consider a wavepacket dynamics whose centre at $t = 0$ has the classical energy $E = 0.25$ for the Hamiltonian $A = 0$. The energy distribution of the sampled trajectories for this particular case has a peak at around $E = 0.25$, as described above. Figure 5 exhibits the time propagation of the resultant correlation function. After some induction time up to $t \sim 150$, during which the magnitude remains of the order of 1, it grows exponentially. It is obvious that the Fourier transform of the above correlation function beyond the induction time is totally meaningless. Hence, we show three spectra taken from the relatively short time intervals; (a) [0, 41], (b) [0, 82], and (c) [0, 164]. In

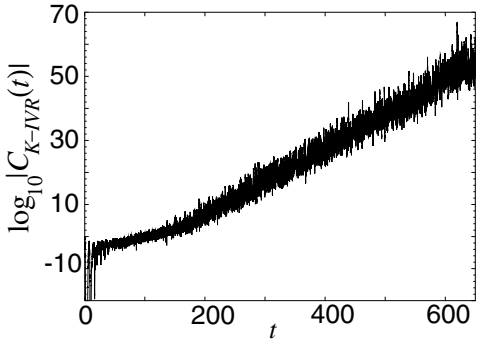

Figure 5. Exponential increase of the correlation function after a short induction time in the case of weak chaos; the Hamiltonian $A = 0.0$ around $E = 0.25$, and $N_t = 10\,000$.

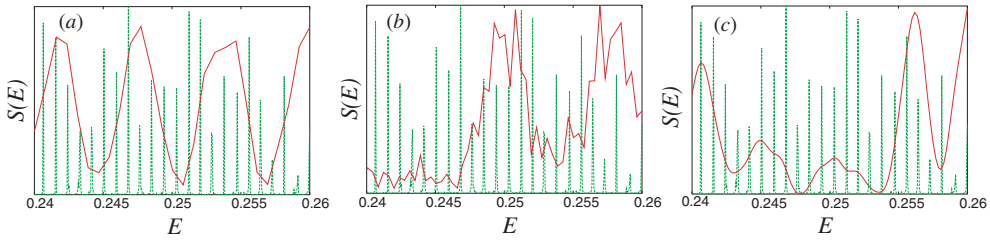

Figure 6. Spectrum taken from the correlation function of figure 5 at the energy around $E = 0.25$. Red and green curves indicate the K-IVR and FQ spectra, respectively. The K-IVR spectra are obtained by the Fourier transform in the interval (*a*) [0, 41] (the resolution $\Delta E = 7.67 \times 10^{-4}$), (*b*) [0, 82] ($\Delta E = 3.84 \times 10^{-4}$) and (*c*) [0, 164] ($\Delta E = 1.92 \times 10^{-4}$).

figure 6, the red and broad spectra represent the K-IVR spectra. The spectrum in green is the FQ spectrum. Although the energy spacing in the FQ spectrum looks quite regular, it actually fluctuates. Comparing the two spectra, the K-IVR directly exposes the difficulty that was mentioned in the introduction. In particular, the spectrum taken from the interval [0, 164] suggests that the present example happens to be extremely tough in that the high-energy trajectories contained in the sampled ensemble seem to have ruined the correlation function entirely. The present example cautions that a direct and naive application of the semiclassical kernel can result in such a poor spectrum. Incidentally, sophisticated methods have been proposed to quantize such weakly chaotic systems (mainly due to the vague tori) [23, 24], most of which can be practically applied only to two-dimensional systems. These methods are not surveyed numerically in this paper. Also, there are some ways to make a partial remedy over the kernel methods; see [11](b), [13], and references therein.

(c) *Strong chaos:* The time propagation of the correlation function is shown in figure 7 and the relevant spectra at around $E = 0.15$ for $A = 0.1$ are displayed in figure 8 again for the time intervals (*a*) [0, 41], (*b*) [0, 82] and (*c*) [0, 164]. Despite the fact that the spectrum looks more irregular in this case than in the above weak chaos, the correlation function of the former increases slightly slower than the latter. Concomitantly, the resultant spectra of figure 8 seem rather better. Nevertheless, it is obvious that the K-IVR fails to give a good resolution.

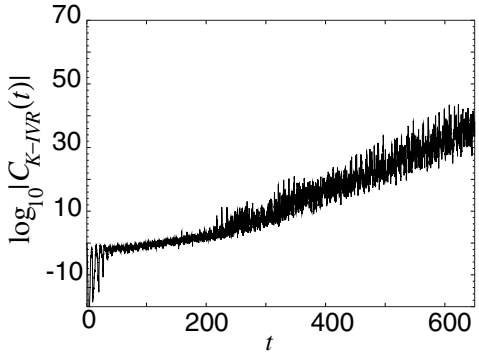

Figure 7. Exponential increase of the correlation function after a short induction time in the case of strong chaos; the Hamiltonian $A = 0.1$ around $E = 0.15$, and $N_t = 10\,000$.

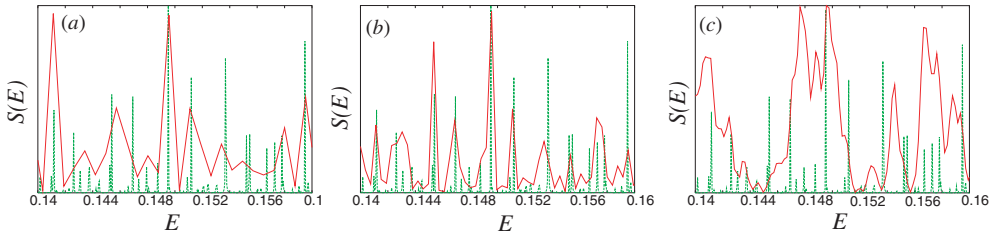

Figure 8. Spectrum taken from the correlation function of figure 7 at the energy around $E = 0.15$. Red and green curves indicate the K-IVR and FQ spectra, respectively. The K-IVR spectra are obtained by the Fourier transform in the interval (*a*) [0, 41] (the resolution $\Delta E = 7.67 \times 10^{-4}$), (*b*) [0, 82] ($\Delta E = 3.84 \times 10^{-4}$) and (*c*) [0, 164] ($\Delta E = 1.92 \times 10^{-4}$).

3.3. Numerical study for AFC-I

We now test the accuracy of the AFC-I spectra. Putting $p_0 = 0$ suffices to generate the turn-back orbits. These are sampled in q_0-space so as to mimic the functional shape of $F(q_0, 0)$ in equation (30) using the importance sampling technique.

(a) *Regular system:* Figure 9 displays the spectrum arising from the AFC-I (in red) and that of the FQ mechanics (in green), for the energy region in which the KAM are overwhelmingly dominant. In what follows, all the AFC spectra should not be compared in their spectral height, since the AFC is already different from the FQ correlation function. Only the spectral positions (energies) should be examined. As seen in figure 9, the AFC-I spectrum is very satisfactory. In this respect, we recall that the EBK condition rests only on the information of phase (action integrals) associated with tori, whereas the Gutzwiller trace formula and the K-IVR seriously take account of the amplitude factor through the stability exponents in addition to the phases, thereby distinguishing regular and chaotic systems. On the other hand, the Schrödinger equation can quantize the energy levels irrespective of classical integrability. Likewise, the calculation of the AFC-I (and AFC-II to be considered in the next section) is performed in terms of the phases alone without distinction of the classical integrability. Therefore, the test of the AFC-I in the regular system is highly non-trivial.

(b) *Weak chaos:* Figure 10 gives the AFC-I and FQ spectra (red and green, respectively) for the weak chaos. It is remarkable that the AFC-I actually yields line spectra at most of the

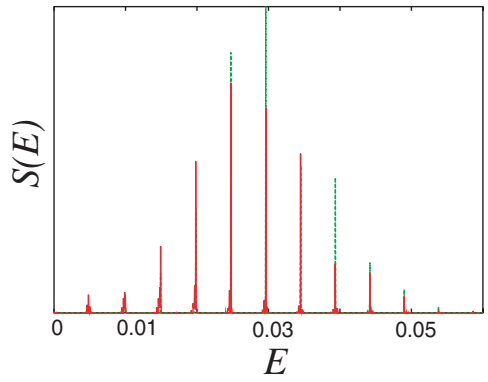

Figure 9. Comparison between the spectra in the regular region with $A = 0.0$ around $E = 0.03$ by AFC-I (in red) and FQ (in green). $T = 655$ (the resolution $\Delta E = 4.79 \times 10^{-5}$) and $N_t = 20\,000$. Only the spectral positions on the energy coordinate should be compared for all the AFC spectra.

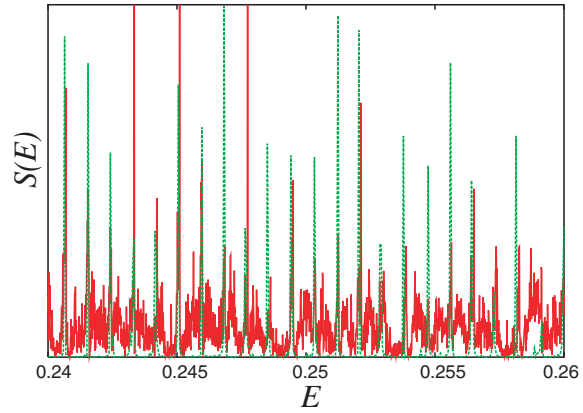

Figure 10. Comparison between the spectra arising from a vague tori with $A = 0.0$ around $E = 0.25$ by AFC-I (in red) and FQ (in green). $T = 655$ (the resolution $\Delta E = 4.79 \times 10^{-5}$) and $N_t = 20\,000$. Only the spectral positions on the energy coordinate should be compared.

correct positions. However, the noise in between the neighbouring spectral lines is not at a negligible level. Trajectories having higher energy may have caused a bad effect in the spectrum as in the case of the K-IVR. The Fourier transform has been performed in the far longer time interval [0, 655] than in the case of the K-IVR, which could not exceed the interval of [0, 200]. The long-time integration has been made possible by the lack of the exponential divergence.

(c) *Strong chaos:* We now challenge the quantization of strong chaos. In contrast to the cases of regular dynamics and weak chaos, it turns out that the AFC-I spectrum is associated with a spectral width despite the fact that the AFC is not associated with the diverging amplitude. To see how the spectral positions are accurate by reducing the effect of such a width, we have squared the AFC-I spectrum (in red) in figure 11. The origin of the width is discussed in the next section. It turns out that most of the spectral peaks are found at the correct positions, but the noise makes spectral identification rather difficult.

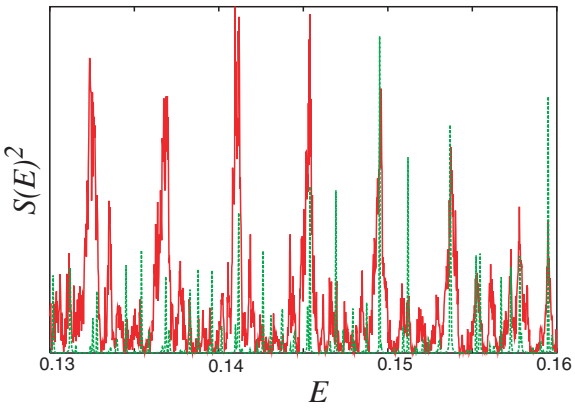

Figure 11. A precise view of the two spectra arising from AFC-I (red) and FQ (green) for $A = 0.1$ around $E = 0.15$ with $T = 655$. The AFC-I spectrum is squared.

Although the progress from the K-IVR is dramatic, one further step is required to improve the spectrum.

4. AFC-II

4.1. Definition of AFC-II

To see the origin of the noise contaminating the AFC-I spectra, we look back at equation (27). In the integral over the initial points q_0, we can apply the stationary phase argument. Then, those trajectories among the turn-back orbits that satisfy

$$\left.\frac{\partial q_t}{\partial q_0}\right|_{p_0=0} \frac{\partial S_1(q_t, q_0, t)}{\partial q_t} - \left.\frac{\partial q_{-t}}{\partial q_0}\right|_{p_0=0} \frac{\partial S_1(q_{-t}, q_0, -t)}{\partial q_{-t}} = 0 \tag{32}$$

should make a major contributions to the integral $\tilde{C}_I(-t, t)$. For the turn-back orbits, it holds that

$$\left.\frac{\partial q_t}{\partial q_0}\right|_{p_0=0} = \left.\frac{\partial q_{-t}}{\partial q_0}\right|_{p_0=0} \tag{33}$$

since $q_t = q_{-t}$ and $p_0 = 0$. Thus the above stationary phase condition is reduced to

$$\frac{\partial S_1(q_t, q_0, t)}{\partial q_t} - \frac{\partial S_1(q_{-t}, q_0, -t)}{\partial q_{-t}} = p_t(q_0, p_0, |t|) - p_{-t}(q_0, p_0, |t|) = 0 \tag{34}$$

which requires that the relevant turn-back orbits should also be periodic orbits ($q_t = q_{-t}$ and $p_t = p_{-t}$) with the period $2t$. Hence, only when t happens to be the one half of the period of the relevant periodic orbits, can $\tilde{C}_I(-t, t)$ have a significant value in the case of a small $\hbar$. Thus, the very accurate integration of equation (27) should be accomplished with the periodic orbits passing through (q_0, p_0) and (q_t, p_t). On the other hand, the noise in the AFC-I might have arisen from the numerical difficulty in treating such an oscillatory integral, in which phase cancellation due to destructive interference among the non-periodic orbits should be performed in a well-balanced manner.

Nonetheless, it is still not a good idea to apply the stationary phase approximation sticking to strict periodic orbits. Therefore, we take a less rigorous (intuitive in a sense) approach. First we recall that the *strict* periodic orbits are required in the limit of $\hbar \to 0$. For the finite

value of the Planck constant, this strict periodicity condition may be relaxed to some extent. So, we can consider the turn-back orbits under a *weakly* periodic boundary condition. The 'weak periodicity' can be efficiently taken into account by means of the following filtering operation, that is, a replacement of the $F^*(q_0, 0)F(q_0, 0)$ in the AFC-I (see equation (27)) as

$$F^*(q_0, 0)F(q_0, 0) \rightarrow |F(q_{2t}, 0)F(q_0, 0)|. \tag{35}$$

The effect of this replacement can be readily understood. Suppose that $F(q_0, 0)$ is sharply localized at a point, say q_X. To represent it, a turn-back orbit should be placed at $q_0 = q_X$ with $p_0 = 0$ ($V(q_X) = E$) at $t = 0$. Then, the function $|F(q_{2t}, 0)F(q_0, 0)|$ becomes very small as soon as the trajectory leaves the point q_X, and becomes large only when it comes back to the same point q_X at time $2t$ ($q_{2t} = q_X$). On the other hand, the relation $V(q_X) = E$ gives $p_{2t} = 0$ uniquely. Hence, this turn-back orbit turns out to be a strict periodic orbit with the period $2t$, since $(q_0, p_0) = (q_{2t}, p_{2t}) = (q_X, 0)$. With this machinery, we can find the periodic orbits within the set of turn-back orbits. In a multi-dimensional system, however, these special orbits can be found only by chance with an extremely small probability. Within this scheme, therefore, we relax the strict periodic orbit condition by letting the function $F(q_0, 0)$ have a finite width in the q_0-space. Thus, the turn-back orbit that comes back to the vicinity of q_X may give a non-zero value to $|F(q_{2t}, 0)F(q_0, 0)|$ with $p_{2t} \simeq 0$. In this way, the turn-back orbits with weak periodicity can be efficiently taken into account, and other orbits are supposed to make a negligible contribution to the quasi-correlation function.

Moreover, for the relevant periodic orbits, it holds that

$$S_1(q_t, q_0, t)|_{p_0=0} - S_1(q_{-t}, q_0, -t)|_{p_0=0} = S_1(q_{2t}, q_0, 2t)|_{p_0=0} \tag{36}$$

and

$$M(q_{-t}, q_t) = M(q_0, q_{2t}) \tag{37}$$

since these are also turn-back orbits. Hence, we define a revised AFC

$$\tilde{C}_{II}(0, 2t) = \int \mathrm{d}q_0 |F(q_{2t}, 0)F(q_0, 0)| \exp\left[\frac{\mathrm{i}}{\hbar} S_1(q_{2t}, q_0, 2t) - \mathrm{i}\frac{\pi}{2} M(q_0, q_{2t})\right] \tag{38}$$

which we call AFC-II. The resultant spectrum can be calculated by the change of variable $2t \rightarrow t$ as

$$S_0(E) = \mathrm{Re} \lim_{T\rightarrow\infty} \frac{1}{T} \int_0^T \mathrm{d}t \int \mathrm{d}q_0 |F(q_t, 0)F(q_0, 0)| \times \exp\left[\frac{\mathrm{i}}{\hbar} S_1(q_t, q_0, t)\Big|_{p_0=0} - \mathrm{i}\frac{\pi}{2} M(q_0, q_t) + \frac{\mathrm{i}}{\hbar} Et\right]. \tag{39}$$

4.2. Numerical study for AFC-II

We now test the AFC-II using the same systems as in the preceding section. The number of turn-back orbits used (N_t) is 20 000, although a very good convergence with respect to N_t seems to be already attained by $N_t = 10\,000$. (Incidentally, N_t for the K-IVR was 10 000, since adding more trajectories in the random sampling made the exponential growth of the correlation function even worse.)

(a) *Regular system:* For the AFC-II, again, only the spectral positions should be compared. Figure 12 shows the AFC-II spectrum (in red), whose spectral positions are indistinguishable from those of the FQ spectrum within the present resolution. We thus have confirmed that K-IVR, AFC-I and AFC-II all yield the correct spectra for the regular system irrespective of the presence of the amplitude factor.

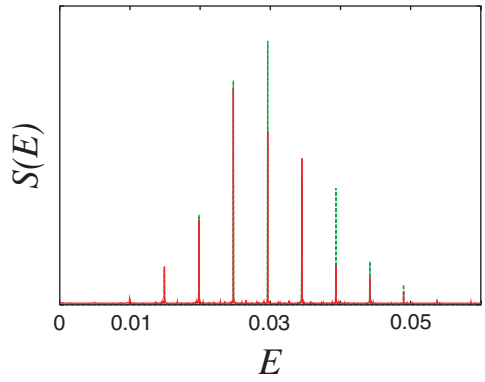

Figure 12. Comparison between the spectra in the regular region with $A = 0.0$ around $E = 0.03$ by AFC-II (in red) and FQ (in green). $T = 655$ and $N_t = 20\,000$. Only the spectral positions on the energy coordinate should be compared.

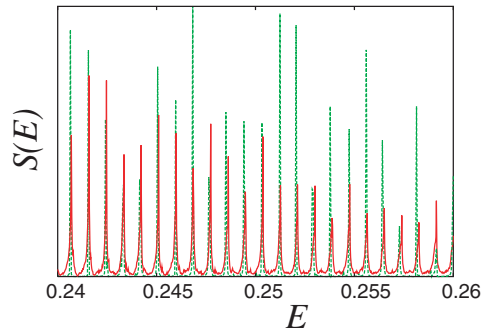

Figure 13. Comparison between the spectra arising from a vague tori with $A = 0.0$ around $E = 0.25$ by AFC-II (in red) and FQ (in green). $T = 1309$ (the FFT resolution $\Delta E = 2.40 \times 10^{-5}$) and $N_t = 20\,000$.

(b) *Weak chaos:* Figure 13 displays a direct comparison of the resultant spectra from the AFC-II (in red) and the FQ (in green). Agreement of the spectral positions between them is excellent. In addition, direct comparison with the AFC-I spectrum (figure 10) demonstrates that the level of the noise is drastically lowered. As noted above, the ensemble of the initially sampled trajectories must include those that have higher energy covering strong chaos, even though the energy $E = 0.25$ of $A = 0$ is mostly in the area of weak chaos. In clear contrast to the K-IVR, nevertheless, the AFC-II turns out to be far less affected by such high-energy components.

(c) *Strong chaos:* We now move on to the system of strong chaos by choosing $A = 0.1$ at the energy $E = 0.15$. Figure 14(a) shows a direct comparison of the resultant spectra by the AFC-II (in red) and the FQ (in green) at the energy around $E = 0.15$, given with $T = 655$. Again, the spectral heights should not be compared. The basic agreement between the two spectra is very good in spite of the fact that the system is extremely chaotic. The noise level and spectral width have been dramatically improved as compared with the spectra for K-IVR (figure 8) and for AFC-I (figure 11). In order to emphasize that the AFC-II is certainly composed of the correct spectral lines, we show its squared spectrum in figure 14(b). Again the semiclassical results are shown in red. The agreement is really remarkable.

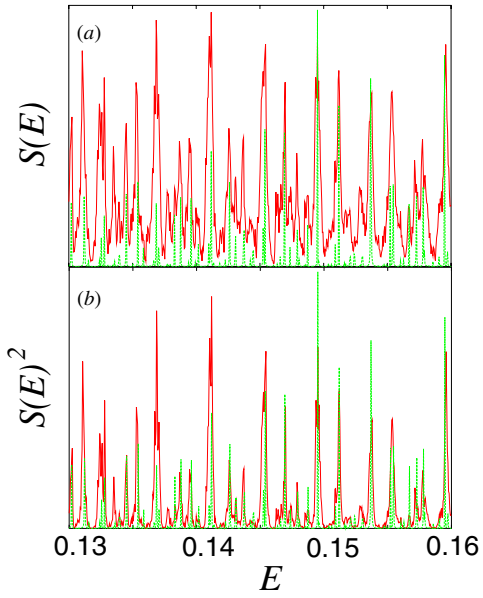

Figure 14. A precise view of the two spectra arising from AFC-II and FQ for $A = 0.1$ around $E = 0.15$ with $T = 655$ (the FFT resolution $\Delta E = 4.79 \times 10^{-5}$) and $N_t = 20\,000$. (*a*) The spectra by AFC-II (in red) and FQ (in green). (*b*) The squared spectrum of AFC (in red) and the original spectrum by FQ (in green).

4.3. On the width of the AFC-II spectrum

Comparing figures 13 and 14, we notice that the latter spectrum is associated with a broader width. At present, the origin of this width is not clear. Obviously, the AFC-II has no mechanism to reflect the diverging property of the amplitude factor. A possible explanation for this is as follows. It is well known that a chaotic trajectory generally visits the close vicinity of many different periodic orbits 'tentatively' (can be long) and changes the hosting periodic orbits from time to time in an irregular manner. For instance, let us suppose that we have a strictly periodic orbit of the period T. Then there must exist a chaotic orbit(s) that may stay very close to this periodic orbit for an interval, say, $[0, 2T]$ and becomes separated 'exponentially' from it. This kind of chaotic orbit, which can be regarded as a weakly periodic orbit, will certainly contribute to the AFC-II, but it also behaves as though it represents a decay-like situation due to the exponential separation. Thus they can bring about a width around the spectral lines. On the other hand, the Gutzwiller periodic orbit theory considers only the strictly periodic orbits, and such a decay-like dynamics in the infinitesimal vicinity of them is taken into account through the eigenvalues of the stability matrix (or the monodromy matrix) in the amplitude factor of the semiclassical Green's function, which correspond to the positive Liapunov exponents. This is common to the K-IVR of equation (4) and can be the origin of the difficulty as stated in equation (4). In contrast, the AFC-II is free of such a diverging amplitude factor, but the phase-space structure of the decaying nature in the vicinity of the periodic orbits is directly taken into account by the turn-back orbits with weak periodicity. Hence, the physical origin of the spectral width seems to be more or less common to all of the AFC-II, the Gutzwiller trace formula and the K-IVR, which seems difficult to avoid in these levels of semiclassical approximation. However, the extent of its quantitative reflection in the

individual theories can be different, and the above numerical results have demonstrated that the width in the AFC-II spectrum is small enough to distinguish individual peaks.

This conjecture cannot be independent of the well-known issue of long-time validity of semiclassical approximation [25] and long-time accuracy of chaotic classical trajectories. Incidentally, we have observed that the accuracy of most of classical trajectories breaks down almost abruptly by the time $T = 655$, which is a technical reason why we stopped the calculation for figure 14 at $T = 655$, where the sixth-order symplectic integrator [22] and the fourth-order locally analytic integrator [26] were used. No significant improvement was achieved by increasing the orders. Note, however, that $T = 655$ is long enough to give a sharp line spectrum for FQ mechanics (shown as green in figure 14). Also, the present conjecture suggests that the choice of the spatial width of $F(q_0, 0)$ should be relevant to control the spectral width. In fact, our preliminary study shows that the width of the AFC-II spectrum varies slightly depending on the breadth of $F(q_0, 0)$. However, the spectral positions do not change practically and are well identified. A much more systematic study is necessary.

5. Concluding remarks

We have proposed the AFC-II and reported that it gives the energy spectrum of classically chaotic systems accurately enough to identify the individual eigenvalues. The trajectories that support standing quantum waves are the turn-back orbits with weak periodicity. On comparing the AFC-II spectra with those of the K-IVR, we may claim that a part of the major difficulty in quantization of chaos has been resolved.

However, we note that there are some classes of dynamics that cannot be quantized in terms of the AFC-II. For instance, there is no non-trivial turn-back orbit in the stadium-billiard. Any point on the flat floor of the stadium with zero momentum is a trivial turn-back orbit, which obviously does not contribute to quantization. (We may be able to remedy this situation by modifying the potential wall so as to have a finite slope.) This type of chaos (boundary-type chaos), in which chaotic motion arises from the boundary condition rather than dynamics, has been extensively studied and is now known to be relevant to the study of electron transport via the quantum dot. On the other hand, we are interested in chaos of molecular systems, in which chaotic nature is acquired along trajectories almost everywhere on the potential function through dynamics itself (dynamics-type chaos). For boundary-type chaos, the Gutzwiller trace formula should work better than for the dynamics-type chaos, since the periodic orbits can be searched in a systematic manner making use of the system symmetry, if any, and since their instability (the positive Liapunov exponent) is not accumulated except at the bouncing on the wall. Even in dynamics of molecules, there are cases in which nontrivial turn-back orbits do not exist, as in the molecular rotation. This aspect will be studied in our future publication.

Another point to be explored more precisely is the canonical invariance of the theory. Recall that the periodic orbits are canonically invariant irrespective of the turn-back boundary condition. Weak periodicity should result in a deviation from the invariance to some extent. To see the canonical invariance more explicitly, we should reformulate the correlation function in momentum representation and see the resultant stationary condition. Also, the theory should be extended so as to treat bound states that include the tunnelling process [27]. These aspects will be studied in future.

Yet, it is certainly a fact that the AFC-II is a very promising method of quantization of chaos (not only chaos but also a wide class of dynamics ranging to regular one). In particular, since the turn-back orbits are easily generated, the AFC-II can be applied to large systems. We are beginning to study chaotic dynamics in those system of realistic size. For instance, we

have already reported a preliminary result of the vibrational spectrum for a cluster composed of seven identical atoms [13] within the AFC-I scheme.

In treating large molecules, the calculation of the Maslov index appears to be a numerically tough problem. In the present paper, it has been computed via the stability matrix, for which $2N \times 2N$ coupled ordinary differential equations have to be integrated in contrast to $2N$ equations for the Hamilton canonical equations of motion. We have figured out a far easier method of the calculation of the Maslov index [28]. Including this material, we will report more detailed characteristics of the AFC-II in the next paper [29].

Acknowledgments

This work has been supported in part by the Grant-in-Aid from the Ministry of Education, Science, and Culture of Japan. We also thank Professor W H Miller and S Takahashi for valuable discussions on the AFC.

References

[1] Tabor M 1989 *Chaos and Integrability in Nonlinear Dynamics* (New York: Wiley)
Reichl L E 1992 *The Transition to Chaos* (New York: Springer)
Nakamura K 1993 *Quantum Chaos* (Cambridge: Cambridge University Press)
Gaspard P 1993 *Chaos, Scattering and Statistical Mechanics* (Cambridge: Cambridge University Press)
[2] Berggren K-F and Åberg S (ed) 2001 *Quantum Chaos Y2K Physica Scripta* (Stockholm, Sweden: The Royal Swedish Academy of Sciences)
[3] Gutzwiller M C 1970 *J. Math. Phys.* **11** 1791
Gutzwiller M C 1971 *J. Math. Phys.* **12** 343
Gutzwiller M C 1990 *Chaos in Classical and Quantum Mechanics* (Berlin: Springer)
[4] Voros A 1988 *J. Phys. A: Math. Gen.* **21** 685
[5] Berry M V and Keating J P 1990 *J. Phys. A: Math. Gen.* **23** 4839
Berry M V and Keating J P 1992 *Proc. R. Soc.* A **437** 151
[6] Vergini E and Wisniacki D A 1998 *Phys. Rev.* E **58** R5225
Vergini E G 2000 *J. Phys. A: Math. Gen.* **33** 4709
[7] Miller W H 1970 *J. Chem. Phys.* **53** 3578
[8] Heller E J 1991 *J. Chem. Phys.* **94** 2723
[9] Sepúlveda M A and Heller E J 1994 *J. Chem. Phys.* **101** 8004
Sepúlveda M A and Grossmann F 1996 *Adv. Chem. Phys.* **96** 191
[10] Campolieti G and Brumer P 1994 *Phys. Rev.* A **50** 997
Provost D and Brumer P 1995 *Phys. Rev. Lett.* **74** 250
[11] Kay K G 1994 *J. Chem. Phys.* **100** 4377
Kay K G 1994 *J. Chem. Phys.* **100** 4432
Kay K G 1994 *J. Chem. Phys.* **101** 2250
[12] Miller W H 1974 *Adv. Chem. Phys.* **25** 69
Schulman L S 1981 *Techniques and Applications of Path Integration* (New York: Wiley)
Gaspard P, Alonso D and Burghardt I 1995 *Adv. Chem. Phys.* **90** 105
[13] Inoue-Ushiyama A and Takatsuka K 2001 *Phys. Rev.* E **64** 056223
[14] Hinde R J, Berry R S and Wales D J 1992 *J. Chem. Phys.* **96** 1376
Hinde R J and Berry R S 1993 *J. Chem. Phys.* **99** 2942
[15] Takatsuka K 2001 *Phys. Rev.* E **64** 016224
[16] Takatsuka K and Inoue A 1997 *Phys. Rev. Lett.* **78** 1404
Inoue-Ushiyama A and Takatsuka K 1999 *Phys. Rev.* A **59** 3256
Inoue-Ushiyama A and Takatsuka K 1999 *Phys. Rev.* A **60** 112
[17] Goldstein H 1980 *Classical Mechanics* (New York: Addison-Wesley)
[18] Miller W H 1974 *Adv. Chem. Phys.* **25** 69
[19] Shao J and Makri N 1999 *J. Phys. Chem.* A **103** 7753
Shao J and Makri N 1999 *J. Phys. Chem.* A **103** 9479
[20] Hashimoto N and Takatsuka K 1995 *J. Chem. Phys.* **103** 6914

[21] Kosloff D and Kosloff R 1983 *J. Comput. Phys.* **52** 35
[22] Yoshida H 1990 *Phys. Lett.* A **150** 262
Takahashi K and Ikeda K 1993 *J. Chem. Phys.* **99** 8680
[23] Jaffé C and Reinhardt W P 1982 *J. Chem. Phys.* **77** 5191
Shirts R B and Reinhardt W P 1982 *J. Chem. Phys.* **77** 5204
[24] Noid D W and Marcus R A 1975 *J. Chem. Phys.* **62** 2119
Swimm R T and Delos J B 1979 *J. Chem. Phys.* **71** 1706
Skodje R T, Borondo F and Reinhardt W P 1985 *J. Chem. Phys.* **82** 4611
Sholberg K and Shirts R B 1994 *J. Chem. Phys.* **101** 7763
Sohlberg K, Tuzun R E, Sumpter B G and Noid D W 1998 *Phys. Rev.* A **57** 906
[25] A crucial argument on this matter is given in Tomsovic S and Heller E J 1991 *Phys. Rev. Lett.* **67** 664
[26] Ushiyama H, Arasaki Y and Takatsuka K 2001 *Chem. Phys. Lett.* **346** 169
[27] Takatsuka K, Ushiyama H and Inoue-Ushiyama A 1999 *Phys. Rep.* **322** 347
[28] Takahashi S and Takatsuka K in preparation
[29] Hotta K, Takahashi S and Takatsuka K unpublished